UC San Diego
UC San Diego Previously Published Works

Title

Zooglider-Based Measurements of Planktonic Foraminifera in the California Current System

Permalink

Journal

ISSN

Authors

Gaskell, Daniel E
Ohman, Mark D
Hull, Pincelli M

Publication Date

DOI

Peer reviewed

ZOOGLIDER-BASED MEASUREMENTS OF PLANKTONIC FORAMINIFERA IN THE CALIFORNIA CURRENT SYSTEM

DANIEL E. GASKELL[1],*, MARK D. OHMAN[2] AND PINCELLI M. HULL[1]

ABSTRACT

Spines and rhizopodia play an important role in the feeding behavior, symbiont ecology, shell geochemistry, and density and drag of planktonic foraminifera. However, there are few empirical data on planktonic foraminifera *in situ*, and these delicate structures are disturbed on capture. Here, we report spine and rhizopod measurements from underwater images obtained in the California Current System near La Jolla, California by *Zooglider*, a new autonomous zooplankton-sensing glider. Across all observed species, we find that spine length and flexibility correlate with test size and that spines increase the effective prey encounter volume of spinose foraminifera by two to three orders of magnitude. Our data also yielded several novel observations regarding hastigerinid foraminifera (*Hastigerinella digitata* and *Hastigerina pelagica*), a group of unusually large planktonic foraminifera that are abundant in our dataset below 250 m. First, the effective encounter volume of hastigerinid foraminifera can be very large: our largest specimen occupies almost 40 cm^3 (about the size of a golf ball), while the median specimen occupies 5.3 cm^3 (about the size of a cherry). Second, the majority of hastigerinid foraminifera in our dataset have asymmetric bubble capsules, which are most frequently oriented with their bubbles on the upward side of the test, consistent with the hypothesis that the bubble capsule is positively buoyant. Third, 16% of hastigerinid foraminifera in our dataset have dispersed bubble capsules with detached bubbles distributed along the spines and rhizopodia, consistent with a regular source of natural disturbance. Taken together, our observations suggest that hastigerinid foraminifera play a larger role as mesopelagic predators in the California Current System than previously recognized.

INTRODUCTION

Many species of planktonic foraminifera are covered in thin calcite spines, along which granular rhizopodia stream (Schiebel & Hemleben, 2017). These spines and rhizopodia play an important role in foraminiferal behavior: most spinose foraminifera prefer zooplankton prey (Schiebel & Hemleben, 2017), which they ensnare and capture on contact with their rhizopodia (Anderson & Bé, 1976; Hemleben et al., 1989, 1991). In the case of *Hastigerina pelagica*, this snaring ability is remarkably efficient, with adhesive rhizopodia quickly enmeshing and invading the prey's shell (Anderson & Bé, 1976). Spines are thus hypothesized to serve as an energetically inexpensive method of in-

creasing the foraminifer's prey encounter probability (Hemleben et al., 1991). In addition to feeding, spines are used to sun symbiotic algae (Schiebel & Hemleben, 2017) and, more speculatively, have been hypothesized to increase hydrodynamic drag (Lipps, 1979; Furbish & Arnold, 1997). Spine morphology is also important for the interpretation of geochemical proxy data from fossil foraminifera; empirical and theoretical work suggests that the physical arrangement of symbionts along spines and rhizopodia may have a significant effect on stable isotope fractionation in symbiotic foraminifera (Spero et al., 1991; Zeebe et al., 1999; Gaskell & Hull, 2018), which forms the basis of numerous geochemical and paleoclimate proxies (Hillaire-Marcel & Vernal, 2007; Ravelo & Hillaire-Marcel, 2007; Katz et al., 2010).

Thus, there is a need to know the extent and configuration of spines and rhizopodia in planktonic foraminifera in their natural context. Yet, *in situ* observations of planktonic foraminifera are rare. Since the advent of modern oceanography, most studies of living planktonic foraminifera have used plankton net tows and culture observations of foraminifera obtained from plankton nets or SCUBA diving (Schiebel & Hemleben, 2017). Spinose foraminifera in particular are best collected by SCUBA diving, as delicate features such as spines are frequently damaged by the nets (Hemleben et al., 1989; Huber et al., 1996), and even those specimens that remain comparatively undamaged often shed or shorten their spines in response to the stress of the tow (Hemleben et al., 1989). Yet, SCUBA collection has been typically limited to the uppermost 2–5 meters of the ocean (Huber et al., 1996) and is rarely practical deeper than 20–30 m. It is also unclear whether specimens that are damaged during collection, but recover in culture, experience any physiological or behavioral changes compared to life in their natural habitat. Culture conditions are at best only an approximation of the foraminifera's native habitat (Hemleben et al., 1989). Published *in situ* observations are mainly descriptions of how foraminifera may be visually identified by SCUBA divers (Bé et al., 1977; Hemleben et al., 1989; Huber et al., 1996) and remotely operated vehicle (ROV) observations of occurrence (Hull et al., 2011).

Underwater sensing technology can help bridge this gap by allowing observation of plankton behavior and distribution *in situ* (e.g., Schulze et al., 1995; Hull et al., 2011; Hosia et al., 2017). Here, we present observations of spinose planktonic foraminifera from a new autonomous buoyancy glider, *Zooglider*, developed by the Instrument Development Group at the Scripps Institution of Oceanography to facilitate imaging of undisturbed zooplankton *in situ* (Ohman et al., 2019; Whitmore et al., 2019). *Zooglider* is based on a modified *Spray* glider and travels by changing its buoyancy to ascend or descend at an average pitch of 16–18° off the horizontal, with average ~~horizontal~~ and horizontal speeds of ~10 cm s^{-1} and ~15 cm s^{-1}, respectively. After descending to approximately 400 m, *Zooglider* alters its buoyancy,

---
[1] Department of Geology & Geophysics, Yale University, 210 Whitney Avenue, New Haven, CT 06511
[2] California Current Ecosystem LTER site, Scripps Institution of Oceanography, University of California San Diego, 9500 Gilman Drive, La Jolla, CA 92093-0218
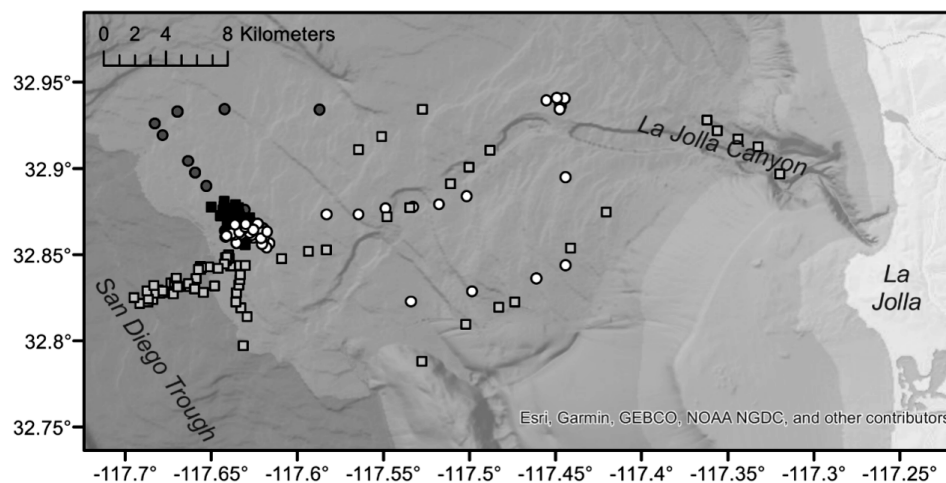* Correspondence author. E-mail: daniel.gaskell@yale.edu

FIGURE 1. Map of *Zooglider* locations in our dataset. White circles represent spring dives (March–May), light gray squares represent summer dives (June–August), dark gray circles represent fall dives (September–November), and black squares represent winter dives (December–February). Bathymetric basemap by Esri (Esri, 2018).

begins gliding back to the surface, and activates a low-power shadowgraph camera that twice per second records zooplankton passing through a low-shear sampling tunnel. Environmental data including temperature, pressure, Chl-*a* fluorescence, and acoustic backscatter are also recorded. *Zooglider* can operate autonomously for up to 50 days while receiving instructions by satellite to direct its course and sampling characteristics. The design and operation of *Zooglider* are described in detail in Ohman et al. (2018) and comparisons with conventional net sampling are reported in Whitmore et al. (2019).

The principal advantages of *Zooglider* are: the scale and quantity of data collected; the high spatial and temporal resolution at which plankton can be measured and correlated with environmental variables; the intentionally low-shear design that minimizes disturbance to delicate structures, such as the fishing tentacles of cnidarians or the rhizopodia of foraminifera; the ability to record orientation of undisturbed specimens; and the autonomous operation of the vehicle. The shadowgraph camera apparatus allows scale to be measured independently of distance from the camera lens and permits imaging of mostly transparent body parts. Multicellular and unicellular zooplankton, such as copepods, ctenophores, acantharians, and foraminifera, can be identified down to about 0.45 mm in diameter (Ohman et al., 2019, figs. 7–8), although resolution is generally insufficient to identify foraminifera to the species level.

Here, we use this technology to address three primary questions:

1. What are the vertical distributions and environmental affinities of the planktonic foraminifera imaged by *Zooglider*?
2. How far do spines and rhizopodia extend in undisturbed spinose foraminifera, and how does this affect the probability of prey encounters?
3. How do the bubble capsules of hastigerinid foraminifera–i.e., *Hastigerinella digitata* (Rhumbler, 1911) and *Hastigerina pelagica* (d'Orbigny, 1839)–

behave in their natural setting, undisturbed by artificial culture conditions?

METHODS

IMAGE COLLECTION

Once images are recovered from *Zooglider*, they are corrected for uneven lighting by flat-fielding and automatically scanned for regions of interest (ROIs) using a two-pass edge-detection algorithm (Ohman et al., 2019). Only ROIs greater than 10 pixels across (or 0.4 mm) are retained. In addition, for the images analyzed here, a size filter was applied that selected images >2 mm equivalent circular diameter. In practice, this means that smaller or non-spinose planktonic foraminifera are not included in the present analysis. Images are classified into broad taxonomic groups by Convolutional Neural Networks (Ellen et al., 2019), and every classification is then verified by a human technician (Ohman et al., 2019).

Our dataset includes a total of 411 individual images of spinose planktonic foraminifera taken over the course of 511 dives from March 2017 to June 2018 on missions we designate as *Zooglider* Rendezvous and San Diego Trough 1–6. The majority of these dives took place in the San Diego Trough (approximately 32°52′N; 117°38′W), with additional dives in surrounding areas, such as La Jolla Canyon (Fig. 1). In a typical dive, approximately 2 m³ of water were imaged by the Zoocam over a diagonal transect of approximately 400 m depth and 600 m surface distance. Dive expeditions were timed to produce an approximately even distribution of dives over all seasons, typically ascending at 3-hour intervals once *Zooglider* reached water >750 m in depth near the San Diego Trough. Representative Zoocam images of foraminifera from the dives are shown in Figure 2.

Environmental data obtained by *Zooglider* and encoded into each image include date, time, latitude/longitude, glider pitch/roll (degrees), pressure (dbar), density (kg m⁻³), salinity (PSU), temperature (°C), and Chl-*a* fluorescence (digital counts). We calculate depth (m) from pressure using a
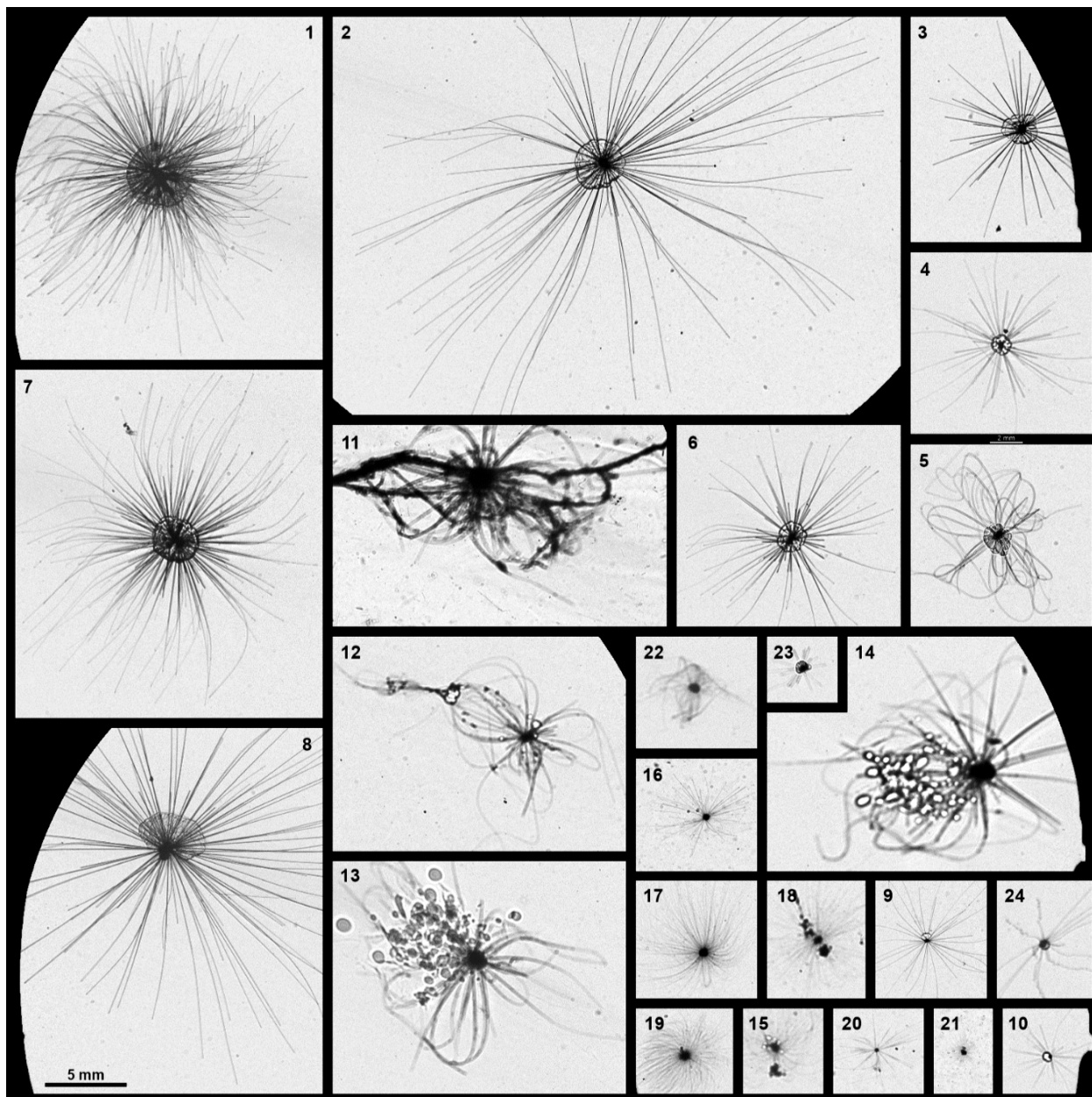
FIGURE 2. Representative images obtained by *Zooglider* from March 2017 to June 2018. **1–8** Hastigerinid foraminifera with intact bubble capsules. **9–15** Hastigerinid foraminifera with dispersed bubble capsules. **16–21** Other spinose foraminifera. **22** Unclear, possibly *G. siphonifera* with tangled rhizopodia or a dispersed hastigerinid that has entirely lost its bubble capsule. **23** Unclear, possibly a small hastigerinid with very short spines. **24** Unclear, possibly a spinose foraminifer with malformed spines. This malformation appears in several other images in our dataset and does not appear to be an artifact of the imaging system. Scale bar = 5 mm.

published conversion accurate to ±0.03 m (Leroy & Parthiot, 1998, eq. 5). Monthly average upwelling index during each dive was taken from the NOAA Pacific Fisheries Environmental Laboratory model (for 33°N, 119°W) in units of cubic meters per second per 100 meters of coastline (PFEL, 2018).

IMAGE PROCESSING

From each image, we measured test major and minor axes, test aspect ratio (defined as the test major axis divided by the test minor axis), minimum spine length, maximum straight spine length, maximum spine/rhizopod length, curved spine/rhizopod length (a rough proxy for rhizopodial extension, defined as the difference between maximum spine/rhizopod length and maximum straight spine length), and estimated number of spines (determined by counting the number of spines in a 90° sector of the spine halo and multiplying by 4). We also obtained the *in situ* vertical orientation of each specimen, corrected for *Zooglider* pitch (Ohman et al., 2019). For hastigerinid foraminifera *Hastigerinella digitata* and *Hastigerina pelagica*, two species with a tropical/subtropical affinity that are distinguished by the presence of a bubble capsule that surrounds the

test (Schiebel & Hemleben, 2017), we also measured minimum capsule radius, maximum capsule radius, capsule diameter, and capsule symmetry coefficient (defined as the minimum capsule radius divided by the maximum capsule radius). All measurements were performed in ImageJ (Schindelin et al., 2012, 2015). Capsule radii and spine lengths were measured from the intersection of the major/minor axis lines (Fig. 3). Because many bubble capsules appeared to be asymmetric (see Results, below), we also estimated the orientation of capsules with a symmetry coefficient <0.75 by drawing a ray from the test midpoint away from the side of the test with the fewest bubbles and correcting the resulting angles for glider pitch so that 0° represented true up. For each image, we also assigned the following categorical variables: foraminiferal type classification (hastigerinid, dispersed, other, or non-foraminifera/unidentifiable); bubble capsule (present/absent); detached bubbles (present/absent); debris adhering to spines/rhizopodia (present/absent); and degree of spine/rhizopod curvature (0 = almost all straight; 1 = some curved, some straight; 2 = almost all curved, but with observable straight segments; 3 = almost no straight segments visible).

Our choice of spine measurements is informed by two limitations of shadowgraph imaging. First, it is difficult to determine the three-dimensional orientation of any given spine, so there is a high likelihood of underestimating length due to perspective. In practice, this means that only the longest spines/rhizopodia can be reliably measured, and measurements of minimum or average spine length are not meaningful. Second, it is difficult to distinguish between rhizopodia and spines. Hastigerinid foraminifera possess uniquely rigid triradiate spines and are known to extend cytoplasmic "fishing lines" from the ends of their spines, a behavior hypothesized to increase their effective encounter volume (Hull et al., 2011). These rhizopodia appear to be visible in our images as long, flexible extensions that continue beyond the straight spines, but the precise demarcation between spine and rhizopod generally cannot be determined from Zoocam images alone. Rhizopodia may extend in an approximately straight, radial arrangement that is difficult to distinguish from spines (e.g., Fig. 2.8) or become entangled with one another (Figs. 2.5, 2.12; see also Hull et al., 2011). This entanglement is distinct from spine flexibility in non-hastigerinid foraminifera, which is captured in the Zoocam images as a gentle curvature typically extending the length of the spine (e.g., Fig. 2.17).

To account for these limitations, we measured: 1) the longest straight spine and 2) the longest spine or rhizopod of any kind. Longest straight spine was measured to the tip of the longest fully-straight spine or to the furthest point before every spine was no longer straight, whichever was furthest. This method likely overestimates the length of the longest straight spine in cases where the rhizopodia are also substantially straight and hence difficult to distinguish from spines, but these data give some indication of the maximum extent of spines and rhizopodia and of the degree of spine flexibility in non-hastigerinid foraminifera. To improve the accuracy of our results, we omitted spine and rhizopod measurements from images we judged to be too small (due to the size of the organism) or too blurry (due to the position of the specimen

TABLE 1. Coefficient of variation (standard deviation divided by mean) of measurements taken from multiple images of the same foraminifera, given as percentages of the original measurements. The calculations for capsule diameter are restricted to the two replicates which possessed an intact bubble capsule.

	C.V.
Major axis	13%
Minor axis	14%
Aspect ratio	18%
Capsule diameter	8%
Shortest spine	17%
Longest straight spine	13%
Longest spine/rhizopod	7%
Number of spines	12%

relative to the camera) to reliably estimate spine length or density.

Fourteen images show the same foraminifer in multiple successive images as determined by timestamp and position in the field of view. In one case, this occurred when *Zooglider* had just reached the nadir point of a dive, changed its buoyancy, and begun its ascent, moving slowly and thus keeping the foraminifer in the camera's field of view for a longer period of time than usual. In the remaining two cases, the foraminifera may have briefly adhered to the camera apparatus, as they remain in the same part of the frame over several successive images while the glider continued to ascend. All three replicated foraminifera were hastigerinids, two with intact bubble capsules and one with a dispersed bubble capsule (see Results, below). These images provide the opportunity to test the replicability of our measurements and the error introduced by viewing angle and movement of the rhizopodia. Measurements were taken on each replicate image using the protocol described above with coefficients of variation as reported in Table 1. In addition, to assess the error introduced by our method of counting spines, ten images were selected at random from the entire dataset and spines were counted along four random 90° sectors of each image. The resulting coefficient of variation was 9%, similar to the errors introduced by viewing angle and movement in the replicates (Table 1). In general, these errors are smaller than the natural variability between similar specimens and therefore should not significantly affect our results.

Images of 400 unique specimens were considered, of which 300 have sufficient resolution to reliably determine spine/rhizopod length and density. Of our specimens, 234 are hastigerinids with intact bubble capsules, 44 are hastigerinids with dispersed bubble capsules, and 122 are other spinose foraminifera. All statistical analyses were performed in R version 3.3.1 (R Core Team, 2016) with packages as cited (Paradis et al., 2004; Canty & Ripley, 2007; Wickham, 2009; Lazaridis, 2014; Sun & Krasnitz, 2014b; Tang et al., 2016; de Vries & Ripley, 2016; Auguie, 2017).

RESULTS

CLASSIFICATION AND MORPHOLOGY

Images usually lack sufficient detail to identify foraminifera to the species level, but three general categories are apparent.
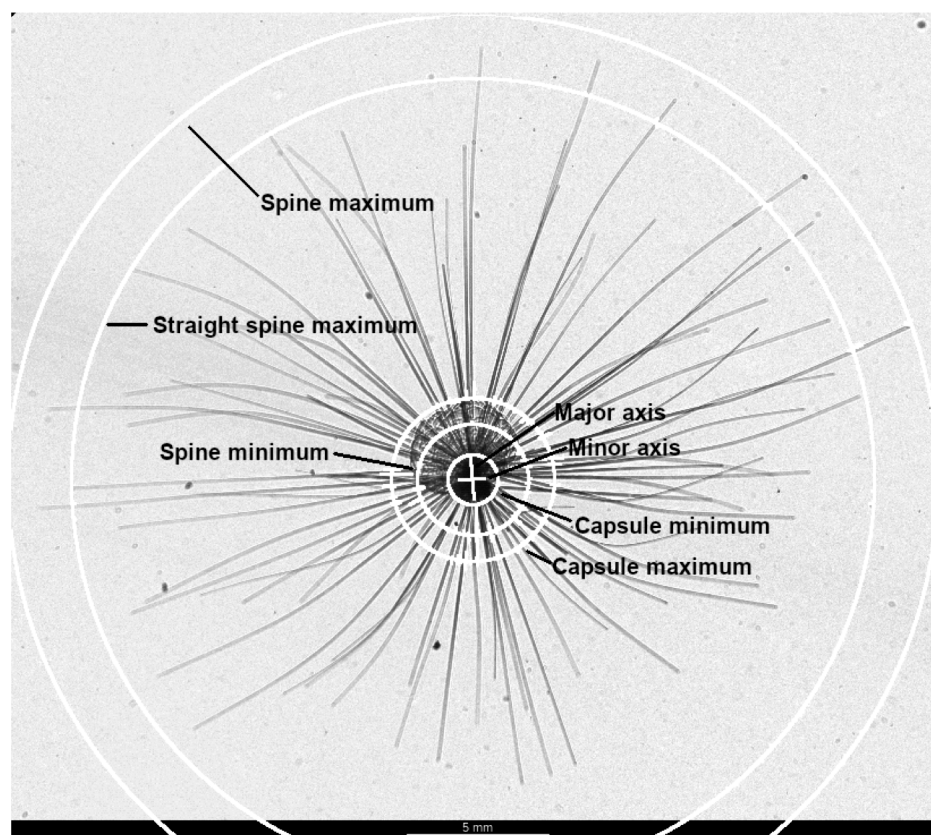
FIGURE 3.   Examples of morphological metrics, measured by expanding circles from the test center point.

Group 1: Intact Hastigerinid Foraminifera

Images of intact hastigerinid foraminifera (Figs. 2.1–2.8) are distinguished by the presence of a prominent bubble capsule surrounding the test, apparently a unique feature of this clade (Murray, 1876; Alldredge & Jones, 1973; Hemleben et al., 1989; Hull et al., 2011). This capsule resembles a nearly transparent mass of spheres or bubbles surrounding the test, through which the spines pass unimpeded. While it is not usually possible to observe test morphology, the clearest hastigerinid images exhibit either a digitate (Fig. 2.7) or globular (Fig. 2.8) morphology. We identify the former as *Hastigerinella digitata* and the latter as the undescribed *Hastigerina* sp. observed by Hull et al. (2011), possibly *H. pelagica* Type IIa (Weiner et al., 2012). The remaining images were not clear enough to distinguish between the two species.

It is notable that a majority (89%) of hastigerinid specimens in our dataset have asymmetric bubble capsules, defined here as a capsule symmetry coefficient of <0.75, with a mean symmetry coefficient of only 0.50. A Gaussian kernel density estimation of our capsule orientation data exhibits a statistically significant peak near 0° ($p < 0.001$), indicating that asymmetric capsules are most likely to be oriented with their bubbles on the upward side of the test (Fig. 4). Absolute capsule angle has weak but significant correlations with capsule symmetry (Pearson $r = 0.31$, $p < 0.01$) and major axis (Pearson $r = -0.23$, $p < 0.01$), indicating that larger foraminifera with less symmetrical capsules are slightly more likely to have capsules with bubbles oriented towards the upward side of the test. Capsule symmetry has a very weak but significant negative correlation with major axis (Pearson $r = -0.15$, $p = 0.02$), indicating that larger foraminifera are slightly less likely to have symmetrical capsules.

Group 2: Dispersed Hastigerinid Foraminifera

Images of dispersed hastigerinid foraminifera (Figs. 2.9–2.15) are distinguished by the presence of detached bubble-like structures scattered along the spines. In most cases, these structures are accompanied by significant curvature or tangling of the spines and rhizopodia, producing a "spaghetti-and-meatballs" appearance.

These images likely represent hastigerinid foraminifera with fragmented bubble capsules, and are referred to here as "dispersed hastigerinids." Dispersed specimens have distributions of test size, depth habitat, and seasonality that are not significantly different from intact hastigerinids, and visual examination reveals a nearly-continuous gradient between hastigerinids with intact and dispersed bubble capsules (Fig. 5). Previous reflected-light images obtained by ROV show similar behavior in the bubble capsules of dispersed hastigerinid foraminifera (Fig. 6). Similar tangling of the spines and rhizopodia can also sometimes be observed in hastigerinid foraminifera with intact bubble capsules (e.g., Fig. 2.5).

Compared to intact hastigerinids, dispersed hastigerinid foraminifera in our dataset have significantly shorter mean
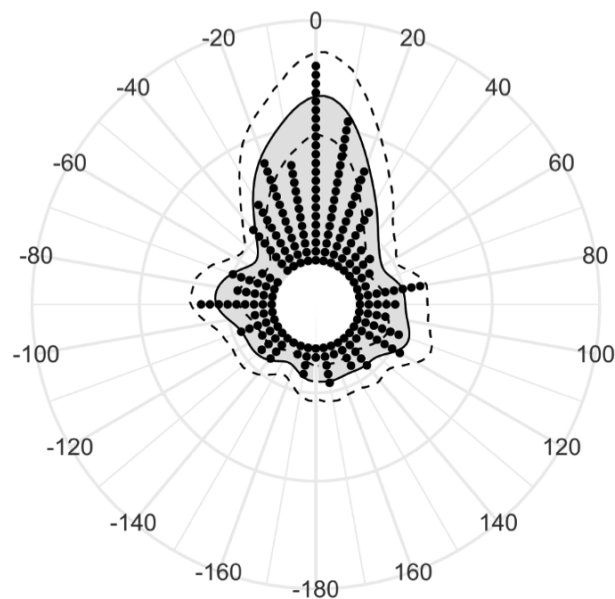
FIGURE 4. Orientation of asymmetric bubble capsules. Black points: histogram of individual measurements in 10° bins. Gray region: Gaussian kernel density estimation with a bandwidth of 10°, scaled to show the predicted density for each bin. Dashed lines: bootstrapped 95% confidence intervals for the kernel density estimation.

length of the longest spine/rhizopod ($p < 0.001$), a significantly shorter mean length of the longest straight spine ($p < 0.001$), and a significantly lower mean number of spines ($p < 0.001$). This observation is robust to size-normalization and occurs across all spine curvature categories (Fig. 7), so it is unlikely to result from overestimation of spine length in intact specimens due to their typically straighter rhizopodia. Thus, our observations likely represent a genuine difference between dispersed and intact specimens.

Group 3: Other Spinose Foraminifera

The remaining images are distinguished by their lack of any visible bubble capsule or bubble capsule fragments (Figs. 2.16–2.24). These images presumably represent a variety of spinose foraminiferal species, but specimens are generally too small relative to the camera resolution to identify species-level differences. To determine if this category could be broken down into statistically distinguishable subgroups

based on morphological traits and environmental occurrence, we applied hierarchical clustering using Euclidean distances and Ward's minimum variance method (Ward, 1963) on a subset of our variables (test major axis, test aspect ratio, spine curvature, size-normalized number of spines, size-normalized maximum straight spine length, size-normalized maximum spine/rhizopod length, depth, fluorescence, and upwelling index). Applying the Tree Branches Evaluated Statistically for Tightness (TBEST) test for the statistical significance of hierarchical cluster branches (Sun & Krasnitz, 2014a) supports the presence of at least three statistically significant clusters ($p < 0.01$), which roughly correspond to A) shallow-dwelling foraminifera concentrated near the deep chlorophyll maximum (DCM); B) deeper-dwelling foraminifera with fewer and straighter spines relative to their test size; and C) deeper-dwelling foraminifera with more spines and spine curvature relative to their test size. For the purposes of the following sections, statistics will be presented both for the category as a whole and for these three statistically generated subcategories.

Morphological Variation

A principal component analysis (PCA) of the morphological variables in our dataset (Fig. 8) shows clear differentiation between intact hastigerinids, dispersed hastigerinids, and other spinose foraminifera. Maximum length of spines and rhizopodia relative to test size load strongly on PC1, test size and the presence and intactness of a bubble capsule load strongly on PC2, and spine curvature loads strongly on PC3 (Table 2). These three components account for 54% of the total morphological variance of the sample.

MEASUREMENTS AND VOLUME OCCUPIED

Summary statistics for each variable and group are given in Table 3. Many morphological variables (including minor axis, spine lengths, capsule diameter, and total number of spines) scale linearly with the major axis of the test, so to facilitate comparison across groups, we calculated size-normalized versions of each capsule and spine variable using the linear regressions shown in Figure 9.

Our results emphasize the large effective volume that hastigerinid foraminifera sweep for prey (Fig. 10). Intact hastigerinid foraminifera range in volume swept from 0.1 cm^3 to almost 40 cm^3, about the size of a golf ball, with a
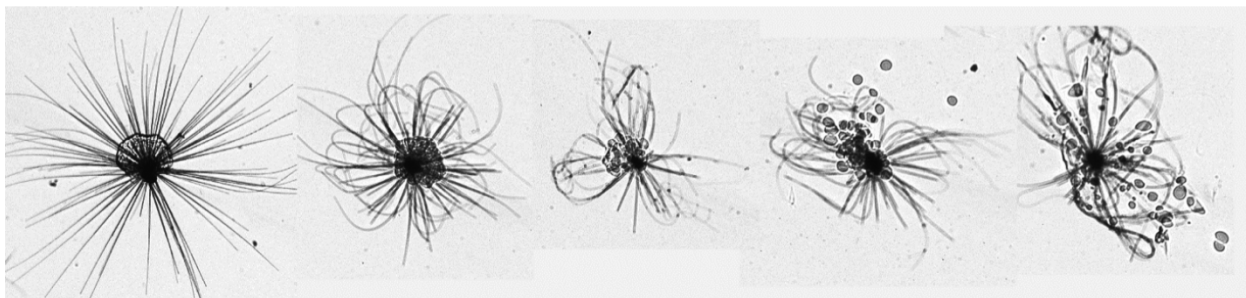

FIGURE 5. Five hastigerinid foraminifera, illustrating the near-continuous gradient from intact bubble capsules (left) to fully dispersed bubbles (right).
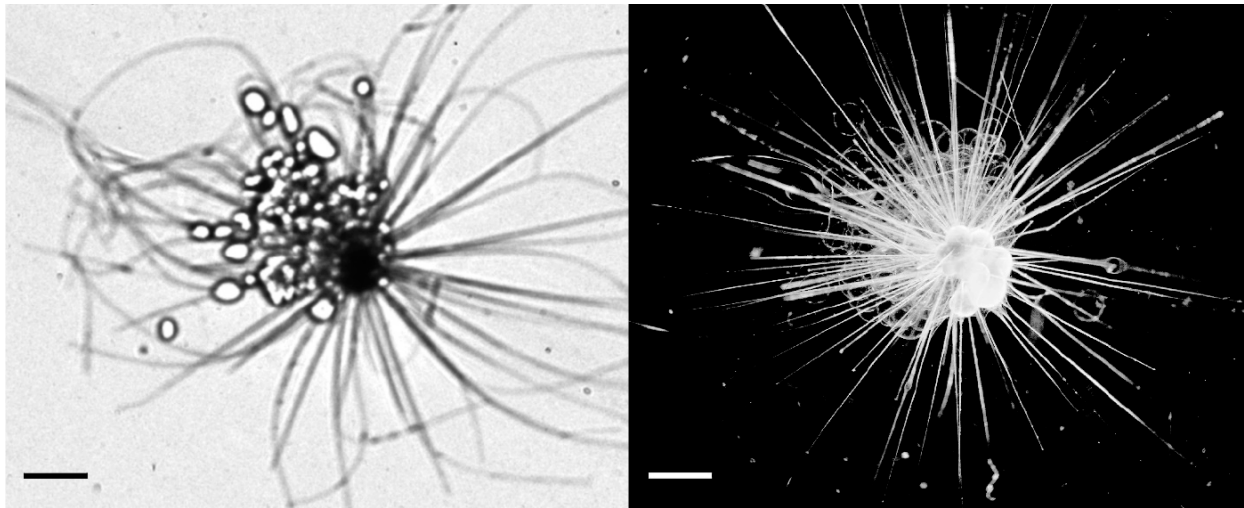
FIGURE 6.   Dispersed hastigerinid foraminifera as shown in silhouette by the Zoocam (left) and under reflected light (right, after Hull et al., 2011, fig. 1B). Contrast has been enhanced in the righthand image to increase the visibility of the bubbles under reflected light. Scale bar = 2 mm.

median volume swept of 5.3 cm³, about the size of a cherry. Dispersed hastigerinid foraminifera sweep a smaller median volume than intact hastigerinid foraminifera of 2.7 cm³, or about the size of a large blueberry (see Discussion, below). By contrast, the majority of non-hastigerinid foraminifera within our dataset sweep a volume of less than 0.5 cm³, or about the size of a pea, with a median volume swept of 0.25 cm³.

ENVIRONMENTAL OCCURRENCE

We find hastigerinid foraminifera primarily below 250 m year-round, with a peak in occurrence in the early part of the upwelling season in April–June (Figs. 11, 12). Other spinose foraminifera are present year-round and at all depths, peaking in occurrence in April at the start of the upwelling season. Unlike in hastigerinid foraminifera, this peak does not continue into our June dives, so it appears to be earlier or shorter than the hastigerinid abundance peak. Deep-dwelling non-hastigerinid foraminifera (deeper than 250 m) appear to occur dominantly during the upwelling season (Fig. 12). Hastigerinid foraminifera show a tendency to peak in occurrence around new moon, while non-hastigerinid foraminifera may peak at either new moon or full moon (Fig. 13). Our statistically identified Cluster 3 shows the strongest evidence for a lunar cycle, peaking shortly after full moon (Fig. 13), although this may reflect their abundance during one set of dives in early April 2018 rather than a true synodic lunar cycle (Fig. 12).

Including images that were unmeasurable due to their position in the field of view, we record one hastigerinid every 1.8 dives (or approximately 3.6 m³ of water) across our entire
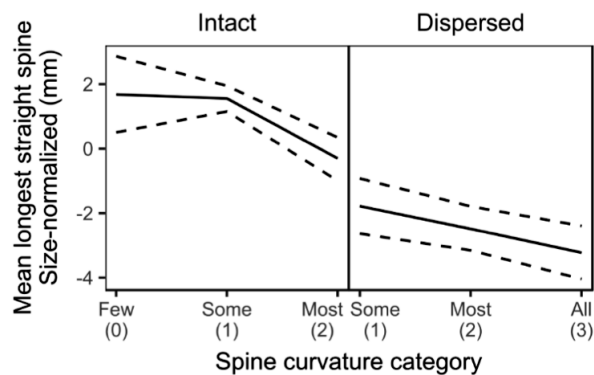

FIGURE 7.   Mean values for longest straight spine broken down by capsule state and spine curvature category, in this case representing how many rhizopodia are visibly curved or tangled. Solid lines connect mean values for each category; dashed lines are bootstrapped 95% confidence intervals for the means.
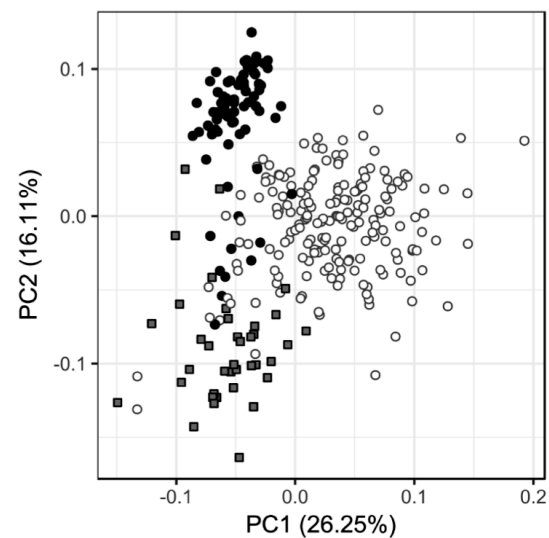

FIGURE 8.   Principal components analysis (PCA) of morphological characters. Symbols follow the three morphological categories defined above: white circles represent hastigerinid specimens with intact bubble capsules, gray squares represent hastigerinid specimens with dispersed bubble capsules, and black circles represent other spinose foraminifera.

TABLE 2. Loadings of morphological variables on the first three principal components. Variables with loadings ≥ |0.50| are in boldface.

	PC1	PC2	PC3
Major axis	0.09	−0.57	0.31
Aspect ratio	0.16	−0.30	0.39
Capsule present	0.27	−0.50	0.03
Capsule is dispersed	−0.23	−0.47	−0.37
Capsule diameter (size-norm.)	0.22	0.05	−0.27
Capsule angle	0.03	−0.05	−0.01
Spine curvature	−0.19	−0.20	−0.57
Spine number (size-norm.)	0.27	0.20	−0.13
Spine minimum (size-norm.)	0.35	−0.12	−0.42
Spine straight max. (size-norm.)	0.53	0.11	0.04
Spine/rhizopod max. (size-norm.)	0.52	0.01	−0.13

sampling period. At peak hastigerinid occurrence, from 250–400 m depth in April–June, we record one hastigerinid every 1.3 dives (or approximately 1.6 m³ of water). Because of selection biases, these numbers (particularly the water-volume estimates) should be considered rough estimates only and likely represent a lower bound for the true abundance of hastigerinids in the California Current System.

DISCUSSION

SPECIES AND ENVIRONMENTAL AFFINITIES

Although regional differences complicate direct comparisons and most net tow studies do not sample below 250 m depth, our occurrence data for all species generally appear consistent with prior observations from the southern California Current System (Sautter & Thunell, 1991; Ortiz et al., 1995; Field, 2004; Hull et al., 2011; Biard & Ohman, in review). We find both morphotypes of hastigerinid foraminifera observed by Hull et al. (2011), with similar patterns of depth and seasonality (Hull et al.,

2011), although the peak in abundance we observe during the upwelling season is shorter than the peak observed by Hull et al. (2011) in Monterey Bay. Likewise, the peak in the abundance of non-hastigerinid foraminifera that we observe in April or May, before the season of greatest upwelling, is consistent with previously reported peaks in non-hastigerinid spinose species, such as *Globigerinella siphonifera* (d'Orbigny, 1839), *Orbulina universa* d'Orbigny, 1839, *Globigerinoides ruber* (d'Orbigny, 1839), *Globigerina bulloides* d'Orbigny, 1826, and *Turborotalita quinqueloba* (Natland, 1938) (Sautter & Thunell, 1991). Several locally abundant species, such as *G. bulloides*, have been observed to favor shallower water during the winter months but expand their range to deeper water (>150 m) during the summer months (Field, 2004), consistent with our observation that deeper-dwelling non-hastigerinid foraminifera are present predominantly during the upwelling season. The environmental and seasonal variables that correlate with these abundances have been examined in detail elsewhere (Kincaid et al., 2000; Field, 2004; Hull et al., 2011; Biard & Ohman, in review).

Our observation that hastigerinid foraminifera may peak in abundance near new moon (Fig. 13) also stands in contrast to prior observations that *H. pelagica* in the Atlantic undergo gametogenesis shortly after full moon (Spindler et al., 1979; Lončarić et al., 2005), as the greatest abundances of large foraminifera in the water column generally occur in the weeks leading up to gametogenesis (Bijma et al., 1990a). This suggests the possibility that the reproductive cycle of California *H. pelagica* may have become offset from the reproductive cycle of Atlantic *H. pelagica*, potentially resulting in reproductive isolation and setting the stage for speciation (Norris, 2000). However, due to uncertainties about the genetic types of *H. pelagica* under consideration and the difficulty of distinguishing *H. pelagica* from *H. digitata* in our data, more data are needed to evaluate this hypothesis.

TABLE 3. Summary mean and standard deviation of morphological variables for intact hastigerinids, dispersed hastigerinids, all other spinose foraminifera, and the three categories defined by the cluster analysis (Cl.1–Cl.3). "SN" indicates a variable that has been size-normalized as described in the text. All lengths are in millimeters.

|	Intact Hast.		Disp. Hast.		All Other		Other (Cl. 1)		Other (Cl. 2)		Other (Cl. 3)	
	n = 238		n = 44		n = 122		n = 25		n = 33		n = 15	
	Mean	*SD*	*Mean*	*SD*	*Mean*	*SD*	*Mean*	*SD*	*Mean*	*SD*	*Mean*	*SD*
Major axis	0.91	0.45	1.11	0.35	0.48	0.15	0.39	0.10	0.51	0.17	0.53	0.09
Minor axis	0.63	0.33	0.82	0.30	0.38	0.13	0.32	0.09	0.40	0.17	0.43	0.08
Aspect ratio	1.46	0.30	1.38	0.24	1.29	0.27	1.21	0.17	1.36	0.36	1.24	0.14
Capsule diameter	2.25	0.98	-	-	-	-	-	-	-	-	-	-
Capsule diameter (SN)	−0.01	0.44	-	-	-	-	-	-	-	-	-	-
Capsule minimum radius	0.72	0.35	-	-	-	-	-	-	-	-	-	-
Capsule maximum radius	1.53	0.73	-	-	-	-	-	-	-	-	-	-
Capsule orientation angle	6.80	84.12	-	-	-	-	-	-	-	-	-	-
Capsule symmetry	0.50	0.18	-	-	-	-	-	-	-	-	-	-
Spine count	58.44	24.57	46.48	10.68	47.82	21.30	44.96	18.41	35.15	14.59	69.00	15.28
Spine count (SN)	2.66	19.56	−14.77	11.63	3.38	20.88	3.47	18.02	−9.69	14.73	23.58	16.40
Spine min length	2.37	1.05	2.36	0.91	0.86	0.30	0.73	0.27	0.95	0.32	0.86	0.25
Spine min length (SN)	0.20	0.82	−0.04	0.80	−0.45	0.26	−0.42	0.26	−0.42	0.26	−0.55	0.25
Spine straight length	7.98	3.29	5.02	1.84	2.87	1.15	2.78	1.04	3.28	1.29	2.13	0.44
Spine straight length (SN)	1.33	2.50	−2.31	1.61	−1.22	1.17	−0.86	1.26	−1.00	1.00	−2.26	0.70
Spine max length	10.79	4.08	8.89	2.98	3.97	1.31	3.33	1.15	4.28	1.53	4.34	0.51
Spine max length (SN)	1.47	3.14	−1.36	2.44	−1.84	1.22	−1.87	1.38	−1.79	1.24	−1.88	0.93
Spine curvature	1.08	0.46	1.79	0.59	1.15	0.58	1.00	0.58	1.00	0.35	2.00	0.00
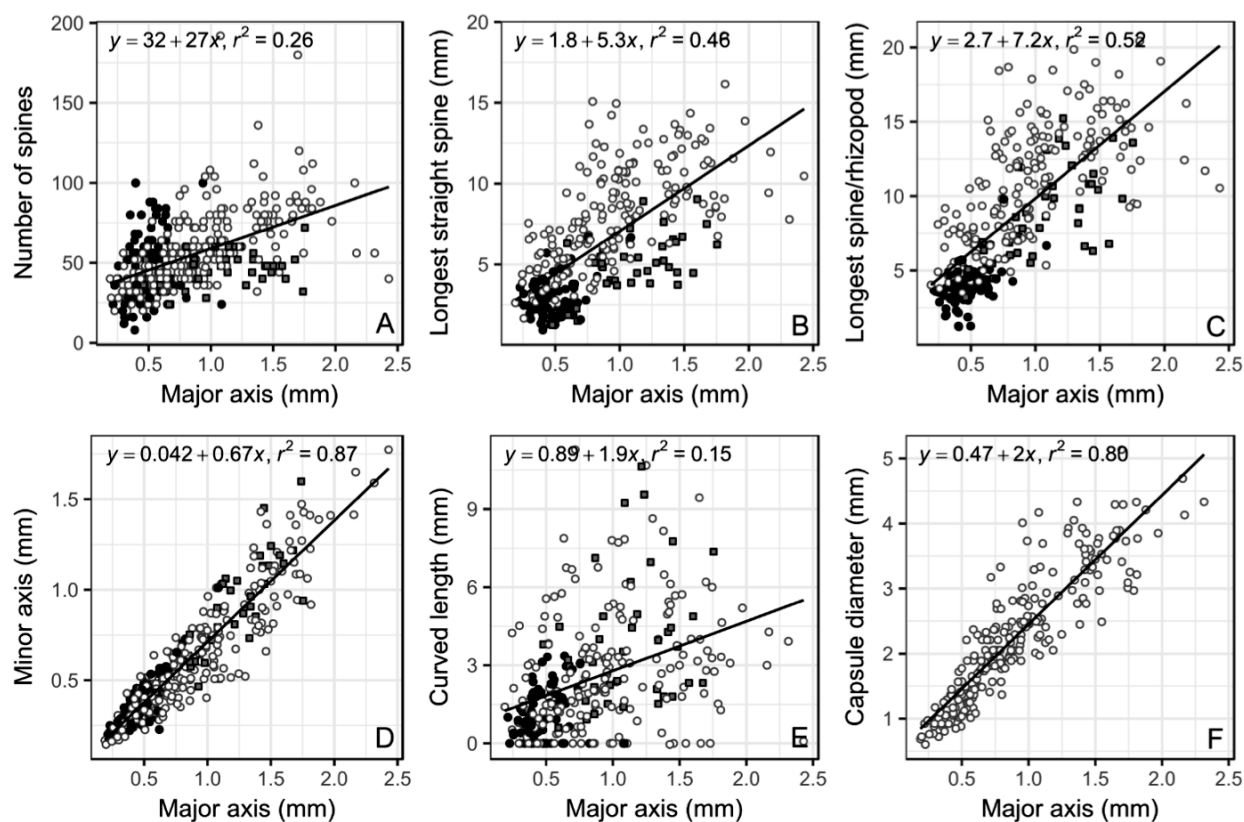
FIGURE 9. Size, spine, and capsule data by major axis, with the ordinary least-squares regression lines used for size-normalization. White circles represent hastigerinid specimens, gray squares represent dispersed hastigerinid specimens, and black circles represent other spinose foraminifera.

The dominant non-hastigerinid species in our dataset is likely *G. bulloides*, which dominates test production in the region by an order of magnitude (Sautter & Thunell, 1991) and exhibits the depth distribution (Field, 2004), size and morphology (Schiebel & Hemleben, 2017), and seasonal bloom patterns (Sautter & Thunell, 1991) observed in our images. In particular, our statistically identified Cluster 3 may be composed primarily of *G. bulloides* given its depth, bloom pattern, and numerous flexible spines (Sautter & Thunell, 1991; Schiebel & Hemleben, 2017). The second most common non-hastigerinid species in our dataset may be *O. universa*, a large, mixed-layer-dwelling spinose species (Schiebel & Hemleben, 2017) that is present in the region year-round (Sautter & Thunell, 1991). *Turborotalita quinqueloba* and *G. ruber* can also be abundant (Sautter & Thunell, 1991; Field, 2004), but may typically be too small (Schiebel & Hemleben, 2017) to be represented in our dataset.

Hastigerinid foraminifera form the majority of our dataset, yet are not reported as common in sediments (Sautter & Thunell, 1991; Field et al., 2006) or tows (Field, 2004) in the southern California Current. This may be explained by: 1) the bias in our dataset toward the very largest species of foraminifera; 2) hastigerinids' uniquely delicate and dissolution-prone tests (Parker & Berger, 1971; Bé et al., 1975); and 3) hastigerinids' deep-depth habitat, which is lower than is typically towed in most net-based studies (see also Biard & Ohman, in review). The delicate nature of *Hastigerina pelagica* has been used to explain prior ob-

servations of discrepancies between tow data and tests in the sediment (e.g., Kipp, 1976). Given the size bias in our images, our data cannot be used to evaluate the relative abundance of shallow and deep-dwelling spinose planktonic foraminifera, but they can be used to assess the absolute occurrence of large hastigerinids in the water column. In this area, our results suggest that hastigerinid foraminifera may play a larger role in mesopelagic ecosystems than previously recognized.

SPINES, RHIZOPODIA, AND PREDATION

Most spinose foraminifera are omnivorous (Anderson et al., 1979; Swanberg & Caron, 1991), but feed dominantly on live zooplankton, particularly copepods (Caron & Bé, 1984; Hemleben et al., 1989; Swanberg & Caron, 1991). Spines are used by spinose planktonic foraminifera to capture and consume zooplankton significantly larger than their own tests by snaring them with their extended rhizopodia (Hemleben et al., 1989). Spines assist in spreading the rhizopodial network, increasing encounter rates for all types of food particles, but also apparently serve a mechanical role in restraining prey. In culture, nonspinose species and spinose foraminifera lacking their spines cannot hold onto moving prey that would be easily captured with the aid of spines (Bijma et al., 1990b; Hemleben et al., 1991).

Our data can be used to quantify how spines increase the food encounter volume of a foraminifer. We are not aware
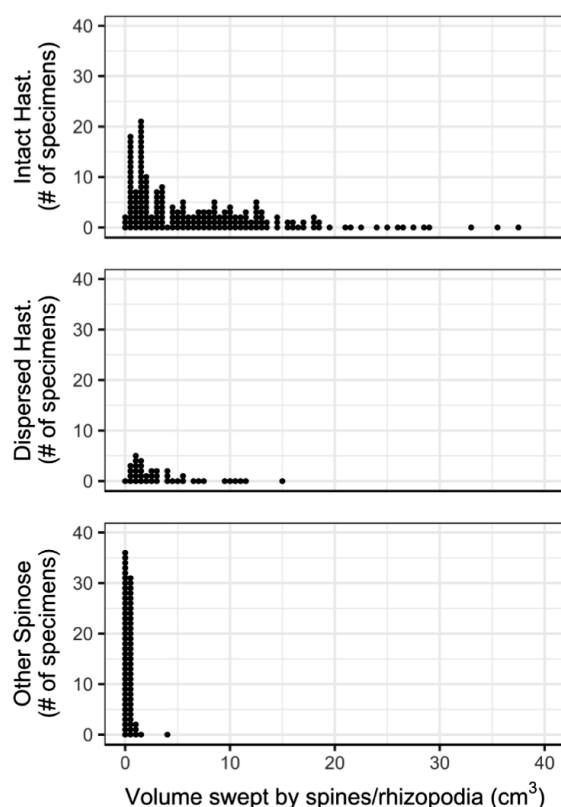
FIGURE 10. Volume of water swept by spines/rhizopodia, in cm³. Panels correspond to the three general categories identified in the text (intact hastigerinids, dispersed hastigerinids, and other spinose foraminifera). Black points: histogram of individual measurements in 0.5 cm³ bins.

of any published measurements of rhizopodial extension in non-spinose foraminifera, but from our observations of cultured specimens (Gaskell; Janet Burke, personal communication, 2018), unsupported rhizopodia do not typically appear to extend more than a full shell-diameter away from a floating foraminifer's test. Using this estimate of 3x shell diameter as a comparison point, growing spines effectively multiplies the volume of water that spinose foraminifera can sweep for prey by a median of 179x for non-hastigerinid foraminifera and 723x for hastigerinid foraminifera. In the most extreme case, one hastigerinid foraminifer in our dataset saw an increase of 10,799x. These volumes are up to an order of magnitude greater than previously published measurements of spine volumes based on cultured specimens: the largest volume previously reported for *Hastigerina pelagica* was 4 cm³ (Alldredge & Jones, 1973), while our largest volume is 37.6 cm³. The volumes of dispersed hastigerinids in our dataset are more consistent with prior reports, perhaps suggesting that the disturbances experienced by foraminifera in culture have a similar mechanical and physiological effect to the forces dispersing foraminiferal capsules in nature. Taken together, our results emphasize the gain in prey encounter potential offered by possessing spines.

It has also been frequently hypothesized that foraminiferal spines evolved to reduce their sinking rate (Lipps, 1979; Haynes, 1981; Furbish & Arnold, 1997; BouDagher-Fadel, 2015). This hypothesis was considered in some detail by

Furbish & Arnold (1997), who found that spines may help decrease the sensitivity of foraminifera to unintended changes in buoyancy, but that–in the case of most real-world spinose foraminifera–cytoplasm-covered spines should not cause a large enough increase in drag to offset the effect of the added mass of calcite (Furbish & Arnold, 1997). Instead, foraminifera primarily self-regulate their buoyancy through the production of lipids and metabolic gases (Furbish & Arnold, 1997; Schiebel & Hemleben, 2017). However, Furbish & Arnold (1997) found that growing fewer and longer spines can be hydrodynamically favorable so long as foraminifera are able to overcome the problem of spine breakage. This strategy may be more attainable for hastigerinid foraminifera than for most other foraminifera due to hastigerinids' uniquely rigid triradiate spines. In this case, the long spines, thin shell, and bubble capsule of hastigerinids may all represent adaptations to increase drag and buoyancy and promote viscous settling. However, the intensive role that spines play in the hunting behavior of spinose foraminifera, and the associated energy tradeoffs involved in maintaining such a large array of spines and rhizopodia, argues strongly that feeding efficiency–rather than drag–is the first-order evolutionary driver behind the development of spines (Hemleben et al., 1991).

BUBBLE CAPSULE BEHAVIOR

Asymmetrical Bubble Capsules

The majority of our hastigerinid specimens exhibit asymmetric bubble capsules, with capsules most likely to be oriented with their bubbles on the upward side of the test (Fig. 4). This is in contrast to prior reports, where intact bubble capsules in captured individuals are often described as spherical (Bé et al., 1977; Hull et al., 2011). This upward-biased asymmetry may represent either the true *in situ* condition of the bubble capsules or a systematic disturbance that occurs as plankton flows through the Zoocam. Evidence against the Zoocam disturbance hypothesis includes: 1) the Zoocam's low-shear design as confirmed by flow dynamic modeling and photographic observation (Ohman et al., 2019; Whitmore et al., 2019; Fig. 2); 2) the lack of detached or "blown off" bubbles around asymmetric capsules; 3) the comparatively minor disturbance of extended rhizopodia; 4) the lack of any obvious hydrodynamic feature of *Zooglider* that might specifically disturb the underside of foraminifera; and 5) the observation that the bubbles are biased towards true up rather than towards the plane of *Zooglider*, which glides at an average pitch of 17° (Ohman et al., 2019). Thus, we suspect that the observed bias in capsule orientation reflects a genuine *in situ* orientation preference rather than a systematic disturbance.

These data are consistent with the hypothesis that the capsule is positively buoyant. Hastigerinid bubble capsules are commonly thought to aid floatation (Bé, 1969; Bé et al., 1977; Spindler et al., 1978; Haynes, 1981; Hemleben et al., 1989). *Hastigerina pelagica* is known to float well in culture and sink to the bottom when its bubble capsule is dispersed (Bé et al., 1977), but this may be unrelated to capsule buoyancy as many species of spinose foraminifera sink when unhealthy or gametogenic and *H. pelagica* has been observed floating without a bubble capsule (Hemleben et al.,
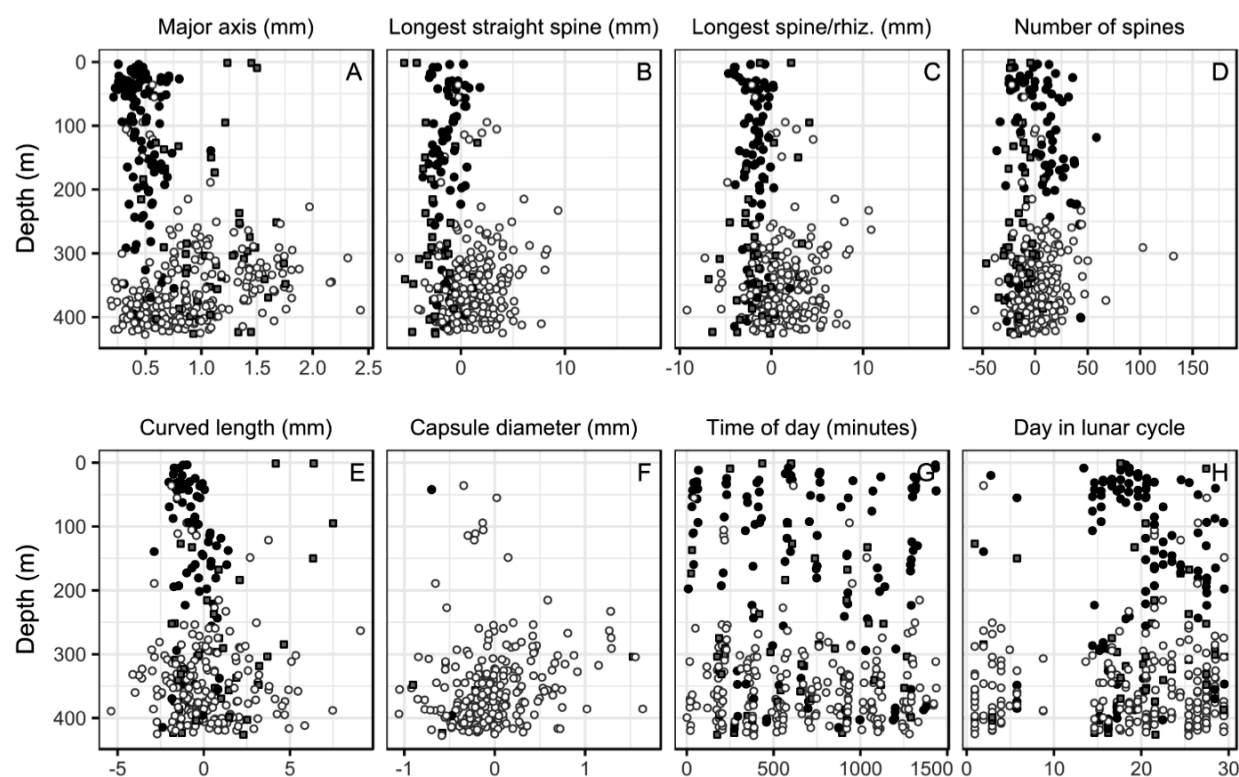
FIGURE 11.   Size, spine, and occurrence data by depth. In panels **B–F**, the x-axis is normalized to shell size using the regressions shown in Figure 9. White circles represent intact hastigerinid specimens, gray squares represent dispersed hastigerinid specimens, and black circles represent other spinose foraminifera. **G** and **H** show occurrence by time of day and day of lunar cycle, respectively, where time 0 is midnight and day 0 is new moon.

1989). Regardless, it is probable that the bubbles are at least mildly buoyant, as foraminiferal cytoplasm must be positively buoyant to offset the negative buoyancy of the heavy calcite test (Hemleben et al., 1989). If this is the case, some combination of the following factors may explain our observations: 1) capsules may naturally become asymmetric due to disturbance (Hull et al., 2011) or poor health (Hemleben et al., 1989), or from a tendency for bubbles to congregate near the aperture; 2) the entire foraminifer may tend to reorient itself under the buoyancy of its capsule; and 3) bubbles may tend to migrate towards the upward side of the test over time.

Our results are the first direct observations of preferential orientation in planktonic foraminifera. Previously, spinose foraminifera have been assumed to lack a preferred orientation based on the symmetry of their spines (Boltovskoy & Wright, 1976), while non-spinose foraminifera may have preferred orientations that are hydrodynamically favorable (Lipps, 1979; Caromel et al., 2014). However, we do not find evidence of preferential orientation of the test itself, as there is no significant correlation between test aspect ratio (a proxy for test orientation with respect to the camera) and either capsule symmetry ($p = 0.81$) or capsule orientation ($p = 0.84$).

Dispersed Bubble Capsules

It is notable that 16% of all hastigerinid specimens in our sample exhibit dispersed bubble capsules, with detached bubbles distributed along the spines and rhizopodia (as in Fig. 6). This is in contrast to prior reports in which hastigerinids *in situ* are presumed to possess intact bubble capsules (Alldredge & Jones, 1973; Bé et al., 1977), with capsule dispersal most frequently associated with tow damage or manipulation in culture (Bé et al., 1977; Hull et al., 2011)–although free-floating *Hastigerina pelagica* without bubble capsules have also been reported (Hemleben et al., 1989). Dispersal is unlikely to be caused by *Zooglider* itself for the reasons given above. In addition, if dispersal were caused by collision with the walls of the sampling tunnel, we would expect dispersed hastigerinids to appear most frequently near the top or bottom of the Zoocam field of view; yet the distribution of dispersed specimens in the Zoocam field of view is not significantly different from the distribution of intact specimens (Kolmogorov-Smirnov test of equality, $p = 0.37$). Thus, our data imply the action of a natural process that regularly disturbs bubble capsules *in situ*. We consider two hypotheses for the origin of this dispersal: disturbance by encounters with prey or other plankton, and gametogenesis.

Feeding and encounters with meso- and macro-plankton are likely to disturb hastigerinids. Eighty-six percent of dispersed hastigerinid specimens have black debris attached to their rhizopodia and spines (as in Fig. 2.12), compared to only 14% of intact hastigerinid specimens; this is a significant difference ($p < 0.001$). If this debris represents captured prey or associated particles, this could support the hypothesis that encounters with prey items account for the dispersed specimens. However, culture observations show that
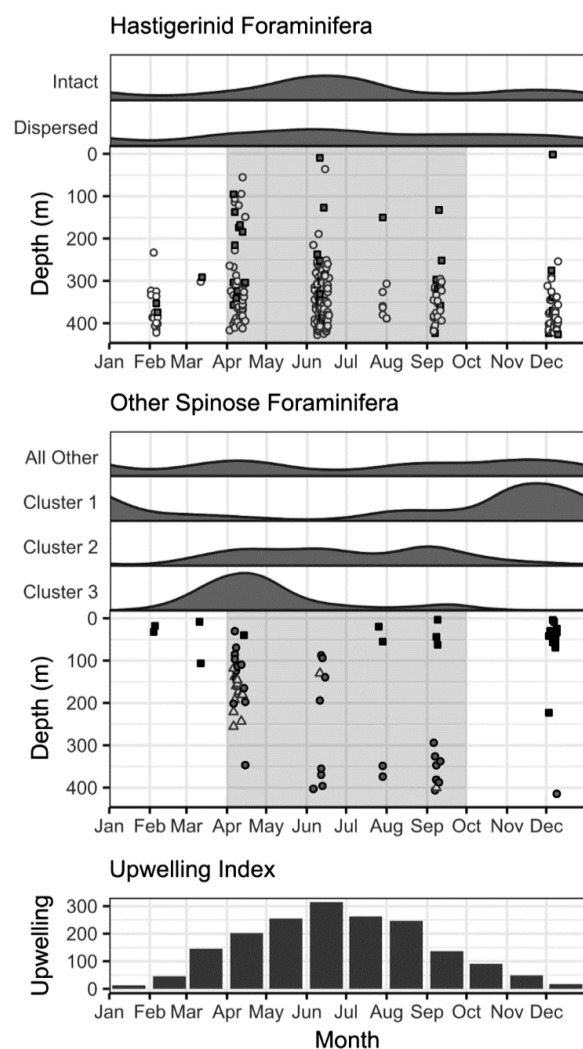
FIGURE 12. Seasonality and depth of specimens. Shaded curves are Gaussian kernel density estimations of seasonal abundance with a bandwidth of one month (30.4 days), standardized for sampling effort by dividing the density estimation of occurrence by the density estimation of dives. Gray shading in the depth plots highlights a typical upwelling season of April–September (e.g., Brady et al., 2017). Top: Hastigerinid foraminifera. White circles represent intact hastigerinid foraminifera; gray squares represent dispersed hastigerinid foraminifera. Middle: Other spinose foraminifera. Shapes indicate the three subcategories assigned by our cluster analysis, above; black squares indicate the thermocline-dwelling cluster (Cluster 1), gray circles indicate the deeper-dwelling cluster with fewer spines (Cluster 2), and white triangles indicate the deeper-dwelling cluster with more spines (Cluster 3). Bottom: Average monthly upwelling for 2016–2017, for reference (PFEL, 2018). Units are cubic meters per second per hundred meters of coastline.
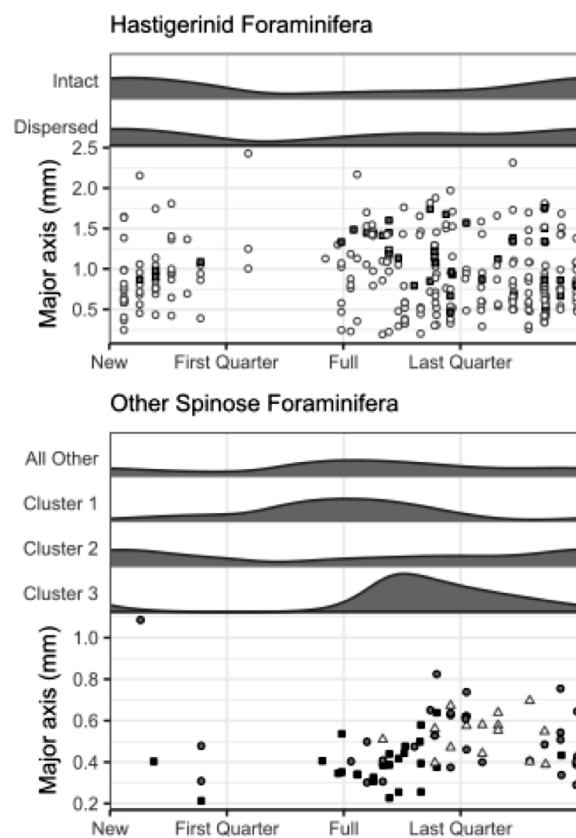

FIGURE 13. Lunar periodicity of abundance (upper gray curves) and test size (major axis of specimens, lower plots with individual symbols). Symbols and effort standardization are as in Figure 12, using a bandwidth of three days for density estimations.

hastigerinids are highly effective hunters that can readily snare and incapacitate prey without dispersing their bubble capsules. Live *Artemia salina* nauplii used as food in culture were snared, incapacitated, and drawn into the bubble capsule without substantially dispersing it (Anderson & Bé, 1976). This suggests that many of the observed dispersal events do not arise from normal feeding, but rather from encounters with larger meso- and macro-plankton which escape or which the foraminifera do not attempt to con-

sume as food. Escaping copepods can travel at over 0.6 m s^{-1} (Kiørboe et al., 2010), with peak forces of 500–600 μN (Lenz et al., 2004), so it is reasonable to assume that such encounters could result in bubble dispersal and rhizopodial tangling like that caused by handling in culture (e.g., Hull et al., 2011).

An alternative hypothesis is gametogenesis. *Hastigerina pelagica* disperses its bubble capsule during gametogenesis (Alldredge & Jones, 1973; Spindler et al., 1978; Hemleben et al., 1979), but this is unlikely to account for the majority of our observations as this event occupies less than 15 hours (Spindler et al., 1978), or ∼2% of the foraminifer's estimated 29-day lifespan (Spindler et al., 1978, 1979). In addition, gametogenesis in *H. pelagica* is synchronized with the full moon (Spindler et al., 1979), and most gametogenic capsule dispersal occurs in the afternoon and evening (Spindler et al., 1978) whereas the hourly and lunar temporal distributions of dispersed hastigerinids in our dataset are not significantly different from the temporal distributions of intact hastigerinids (Fig. 11G,H; two-sample Kolmogorov-Smirnov, $p > 0.28$ in all cases). Subsequent so-called "spherical bodies" released during gametogenesis are too small (10–30 μm) and are released after the foraminifer has already lost its spines (Spindler et al., 1978).

Foraminifera with dispersed bubble capsules have significantly lower mean number of spines and mean spine

length compared to intact hastigerinid foraminifera (see Results, above). Both of these phenomena may result from spines breaking during the same disturbance that disperses the bubble capsule. When disturbed, *H. pelagica* may also preferentially break or shorten its spines down to the approximate point of contact with the bubble capsule (Bé et al., 1977; Hull et al., 2011), from which point the spines subsequently regrow in a thinner and more delicate form (JAMSTEC; Bé et al., 1977). While the mean length of the longest spine in dispersed specimens is still significantly longer than mean capsule radius ($p < 0.001$), it is possible that this shortening process, or weak points created by spine repair, may contribute to the shortening of and disappearance of spines after capsule dispersal. Spine shedding during gametogenesis is unlikely to explain observations, as gametogenesis entails the shedding of complete spines by resorption close to their bases, rather than progressive shortening (Spindler et al., 1978; Hemleben et al., 1979).

CONCLUSION

Our data confirm the utility of *Zooglider* for measuring spinose foraminifera and represent the first population-scale measurements of spine, rhizopod, and bubble capsule morphology *in situ*. We find that spines and rhizopodia typically extend ~10 times the diameter of the test in hastigerinid foraminifera and ~8 times the diameter of the test in non-hastigerinid foraminifera. These spine and rhizopod lengths increase the volume occupied by the foraminifer by two to three orders of magnitude over what would be possible without spines, markedly increasing prey encounter probabilities. In addition, we find the first evidence suggestive of a preferential orientation in the water column, with bubbles on hastigerinid species tending to aggregate on the upward side of the test. We also find evidence suggestive of relatively frequent organism-disturbing encounters that result in shortened spines, tangled rhizopodia, and dispersed bubbles in hastigerinid foraminifera. Our data will assist future ecological modeling efforts and inform our understanding of foraminiferal behavior in culture versus *in situ*.

Our results also emphasize the novelty and ecological importance of the hastigerinid life habit. Hastigerinids' unique morphological traits, including bubble capsules and few long and rigid spines, may enable them to remain neutrally buoyant while hunting for prey over a volume of water orders of magnitude larger than that occupied by any other species of planktonic foraminifera. This likely contributes to the success of hastigerinid foraminifera as predators in the deeper waters of the California Current System, where prey such as copepods are less abundant (Ohman et al., 1998). Our results suggest that hastigerinid foraminifera may play a larger role as mesopelagic predators in the California Current System than has been previously recognized.

ACKNOWLEDGMENTS

REFERENCES

Alldredge, A. L., and Jones, B. M., 1973, *Hastigerina pelagica*: Foraminiferal habitat for planktonic dinoflagellates: Marine Biology, v. 22, p. 131–135, doi:10.1007/BF00391777.

Anderson, O. R., and Bé, A. W. H., 1976, A cytochemical fine structure study of phagotrophy in a planktonic foraminifer, Hastigerina pelagica (d'Orbigny): Biological Bulletin, v. 151, p. 437–449, doi:10.2307/1540498.

Anderson, O. R., Spindler, M., Bé, A. W. H., and Hemleben, C., 1979, Trophic activity of planktonic foraminifera: Journal of the Marine Biological Association of the United Kingdom, v. 59, p. 791–799, doi:10.1017/S002531540004577X.

Auguie, B., 2017, gridExtra: Miscellaneous functions for "grid" graphics. Available from https://CRAN.R-project.org/package = gridExtra

Bé, A.W.H., 1969, Microstructural evidence of the close affinity of *Globigerinella* Cushman to *Hastigerina* Thomson, *in* Brönnimann, P. and Renz, H.H. (eds.), Proceedings of the First International Conference on Planktonic Microfossils, Geneva 1967: Brill Archive, p. 86.

Bé, A. W. H., Morse, J. W., and Harrison, S. M., 1975, Progressive dissolution and ultrastructural breakdown of planktonic foraminifera, in Sliter, W. V. et al. (eds.), Dissolution of deep-sea carbonates: Cushman Foundation for Foraminiferal Research, Special Publication no. 13, p. 27–55.

Bé, A. W. H., Hemleben, C., Anderson, O. R., Spindler, M., Hacunda, J., and Tuntivate-Choy, S., 1977, Laboratory and field observations of living planktonic foraminifera: Micropaleontology, v. 23, p. 155–179, doi:10.2307/1485330.

Bijma, J., Erez, J., and Hemleben, C., 1990a, Lunar and semi-lunar reproductive cycles in some spinose planktonic foraminifers: Journal of Foraminiferal Research, v. 20, p. 117–127, doi:10.2113/gsjfr.20.2.117.

Bijma, J., Faber, W. W., and Hemleben, C., 1990b, Temperature and salinity limits for growth and survival of some planktonic foraminifers in laboratory cultures: Journal of Foraminiferal Research, v. 20, p. 95–116, doi:10.2113/gsjfr.20.2.95.

Boltovskoy, E., and Wright, R., 1976, Planktonic foraminifera, *in* Boltovskoy, E., and Wright, R. (eds.), Recent Foraminifera: Springer Netherlands, Dordrecht, p. 159–195, doi:10.1007/978-94-017-2860-7_7.

BouDagher-Fadel, M., 2015, Biostratigraphic and Geological Significance of Planktonic Foraminifera, Second Edition: UCL Press, London, 306 p.

Brady, R. X., Alexander, M. A., Lovenduski, N. S., and Rykaczewski, R. R., 2017, Emergent anthropogenic trends in California Current upwelling: Geophysical Research Letters, v. 44, p. 5044–5052, doi:10.1002/2017GL072945.

Canty, A., and Ripley, B. D., 2007, Boot: Bootstrap R (S-Plus) functions.

Caromel, A. G. M., Schmidt, D. N., Phillips, J. C., and Rayfield, E. J., 2014, Hydrodynamic constraints on the evolution and ecology of planktic foraminifera: Marine Micropaleontology, v. 106, p. 69–78, doi:10.1016/j.marmicro.2014.01.002.

Caron, D. A., and Bé, A. W., 1984, Predicted and observed feeding rates of the spinose planktonic foraminifer *Globigerinoides sacculifer*: Bulletin of Marine Science, v. 35, p. 1–10.

de Vries, A., and Ripley, B. D., 2016, ggdendro: Create dendrograms and tree diagrams using "ggplot2". Availablel from https://CRAN.R-project.org/package = ggdendro

d'Orbigny, A., 1839, Voyage dans l'Amérique méridionale: Foraminifera (tome 5 partie 5): Levrault, Strausburg, France, v. 5, 27 p.

Ellen, J. S., Graaf, C. A., and Ohman, M. D., 2019, Improving plankton image classification using context metadata: ~~Journal of Plankton Research (in press)~~.

Esri, 2018, World Ocean Base [basemap]. Scale not given. Available from http://www.arcgis.com/home/item.html?id = 1e126e7520f9466c9ca28b8f28b5e500/ (accessed November 2018).

Field, D. B., 2004, Variability in vertical distributions of planktonic foraminifera in the California Current: Relationships to vertical ocean structure: Paleoceanography, v. 19, doi:10.1029/2003PA000970.

Field, D. B., Baumgartner, T. R., Charles, C. D., Ferreira-Bartrina, V., and Ohman, M. D., 2006, Planktonic foraminifera of the California Current reflect 20th-century warming: Science, v. 311, p. 63–66, doi:10.1126/science.1116220.

Furbish, D. J., and Arnold, A. J., 1997, Hydrodynamic strategies in the morphological evolution of spinose planktonic foraminifera: Geological Society of America Bulletin, v. 109, p. 1055–1072.

Gaskell, D. E., and Hull, P. M., 2018, Morphological controls on vital effects can explain high $\delta^{13}C$ in muricate foraminifera, *in* FORAMS 2018: International Symposium on Foraminifera, June 2018, Edinburgh, UK.

Haynes, J. R., 1981, Foraminifera: Palgrave Macmillan, UK.

Hemleben, C., Bé, A. W. H., Spindler, M., and Anderson, O., 1979, "Dissolution" effects induced by shell resorption during gametogenesis in *Hastigerina pelagica* (d'Orbigny): Journal of Foraminiferal Research, v. 9, p. 118–124, doi:10.2113/gsjfr.9.2.118.

Hemleben, C., Spindler, M., and Anderson, O. R., 1989, Modern Planktonic Foraminifera: Springer-Verlag, New York, 363 p.

Hemleben, C., Mühlen, D., Olsson, R. K., and Berggren, W. A., 1991, Surface texture and the first occurrence of spines in planktonic foraminifera from the early Tertiary: Geologisches Jahrbuch, v. A 128, p. 117–146.

Hillaire-Marcel, C., and de Vernal, A., 2007, Proxies in Late Cenozoic Paleoceanography: Elsevier, Amsterdam, The Netherlands, 862 p.

Hosia, A., Falkenhaug, T., Baxter, E. J., and Pagès, F., 2017, Abundance, distribution and diversity of gelatinous predators along the northern Mid-Atlantic Ridge: A comparison of different sampling methodologies: PLoS ONE, v. 12, doi:10.1371/journal.pone.0187491.

Huber, B. T., Bijma, J., and Spero, H. J., 1996, Blue-water scuba collection of planktonic foraminifera, *in* Lang, M. A., and Baldwin, C. C. (eds.), Methods and Techniques of Underwater Research: Proceedings of the American Academy of Underwater Sciences Scientific Diving Symposium, Smithsonian Institution, Washington, D.C., p. 236.

Hull, P. M., Osborn, K. J., Norris, R. D., and Robison, B. H., 2011, Seasonality and depth distribution of a mesopelagic foraminifer, <mark>Hastigerinella digitata</mark>, in Monterey Bay, California: Limnology and Oceanography, v. 56, p. 562–576, doi:10.4319/lo.2011.56.2.0562.

JAMSTEC *Hastigerina pelagica* (d'Orbigny), 1839: Image database of planktonic foraminifera, Japan Agency for Marine-Earth Science and Technology. Available from http://www.jamstec.go.jp/res/ress/kimopy/foraminifera/e/H_pelagica/ (accessed November 2018).

Katz, M. E., Cramer, B. S., Franzese, A., Hönisch, B., Miller, K. G., Rosenthal, Y., and Wright, J. D., 2010, Traditional and emerging geochemical proxies in foraminifera: Journal of Foraminiferal Research, v. 40, p. 165–192, doi:10.2113/gsjfr.40.2.165.

Kincaid, E., Thunell, R. C., Le, J., Lange, C. B., Weinheimer, A. L., and Reid, F. M., 2000, Planktonic foraminiferal fluxes in the Santa Barbara Basin: Response to seasonal and interannual hydrographic changes: Deep Sea Research Part II: Topical Studies in Oceanography, v. 47, p. 1157–1176.

Kiørboe, T., Andersen, A., Langlois, V. J., and Jakobsen, H. H., 2010, Unsteady motion: Escape jumps in planktonic copepods, their kinematics and energetics: Journal of The Royal Society Interface, v. 7, p. 1591–1602, doi:10.1098/rsif.2010.0176.

Kipp, N. G., 1976, New transfer function for estimating past sea-surface conditions from sea-bed distribution of planktonic foraminiferal assemblages in the North Atlantic, *in* Cune, R. M., and Hays, J. D. (eds.), Investigation of Late Quaternary Paleoceanography and Paleoclimatology: Geological Society of America, v. 145, p. 3–42, doi:10.1130/MEM145-p3.

Lazaridis, E., 2014, lunar: Lunar phase & distance, seasons and other environmental factors. Available from http://statistics.lazaridis.eu

Lenz, P. H., Hower, A. E., and Hartline, D. K., 2004, Force production during pereiopod power strokes in *Calanus finmarchicus*: Journal of Marine Systems, v. 49, p. 133–144, doi:10.1016/j.jmarsys.2003.05.006.

Leroy, C. C., and Parthiot, F., 1998, Depth-pressure relationships in the oceans and seas: The Journal of the Acoustical Society of America, v. 103, p. 1346–1352, doi:10.1121/1.421275.

Lipps, J. H., 1979, Ecology and paleoecology of planktic foraminifera, *in* Foraminiferal Ecology and Paleocology: SEPM (Society for Sedimentary Geology), doi:10.2110/scn.79.06.

Lončarić, N., Brummer, G.-J. A., and Kroon, D., 2005, Lunar cycles and seasonal variations in deposition fluxes of planktic foraminiferal shell carbonate to the deep South Atlantic (central Walvis Ridge): Deep Sea Research Part I: Oceanographic Research Papers, v. 52, p. 1178–1188, doi:10.1016/j.dsr.2005.02.003.

Murray, J., 1876, II. Preliminary reports to Professor Wyville Thomson, F. R. S., director of the civilian scientific staff, on work done on board the "Challenger": Proceedings of the Royal Society of London, v. 24, p. 471–544, doi:10.1098/rspl.1875.0067.

Norris, R. D., 2000, Pelagic species diversity, biogeography, and evolution: Paleobiology, v. 26, p. 236–258.

Ohman, M. D., Drits, A. V., Clarke, M. E., and Plourde, S., 1998, Differential dormancy of co-occurring copepods: Deep Sea Research Part II: Topical Studies in Oceanography, v. 45, p. 1709–1740, doi:10.1016/S0967-0645(98)80014-3.

Ohman, M. D., Davis, R. E., Sherman, J. T., Grindley, K. R., Whitmore, B. M., Nickels, C. F., and Ellen, J. S., 2019, *Zooglider*: An autonomous vehicle for optical and acoustic sensing of zooplankton: Limnology and Oceanography: Methods, v. 17, p. 69–86, doi:10.1002/lom3.10301.

Ortiz, J. D., Mix, A. C., and Collier, R. W., 1995, Environmental control of living symbiotic and asymbiotic foraminifera of the California Current: Paleoceanography, v. 10, p. 987–1009, doi:10.1029/95PA02088.

Paradis, E., Claude, J., and Strimmer, K., 2004, APE: Analyses of phylogenetics and evolution in R language: Bioinformatics, v. 20, p. 289–290.

Parker, F. L., and Berger, W. H., 1971, Faunal and solution patterns of planktonic Foraminifera in surface sediments of the South Pacific: Deep Sea Research and Oceanographic Abstracts, v. 18, p. 73–107, doi:10.1016/0011-7471(71)90017-9.

PFEL, 2018, Monthly index values for all 15 positions (1946–present), Retrieved from: https://www.pfeg.noaa.gov/products/PFEL/modeled/indices/upwelling/NA/data_download.html (accessed October 2018).

R Core Team, 2016, R: A language and environment for statistical computing: R Foundation for Statistical Computing, Vienna, Austria, https://www.R-project.org/.

Ravelo, A. C., and Hillaire-Marcel, C., 2007, The use of oxygen and carbon isotopes of foraminifera in paleoceanography, *in* Hillaire-Marcel, C. and de Vernal, A. (eds.), Proxies in Late Cenozoic Paleoceanography: Developments in Marine Geology, v. 1: Elsevier, Amsterdam, The Netherlands, 862 p.

Rhumbler, L., 1911, Die Foraminiferen (Thalamophoren) der Plankton Expedition; Teil 1-Die allgemeinen Organisationsverhältnisse der Foraminieren, Plankton Expedition Humbold-Stiftung: Kiel and Leipzig, 331 p.

Sautter, L. R., and Thunell, R. C., 1991, Planktonic foraminiferal response to upwelling and seasonal hydrographic conditions; Sediment trap results from San Pedro Basin, Southern California Bight: Journal of Foraminiferal Research, v. 21, p. 347–363, doi:10.2113/gsjfr.21.4.347.

Schiebel, R., and Hemleben, C., 2017, Planktic Foraminifers in the Modern Ocean: Springer, Berlin, 358 p.

Schindelin, J., Arganda-Carreras, I., Frise, E., Kaynig, V., Longair, M., Pietzsch, T., Preibisch, S., Rueden, C., Saalfeld, S., Schmid, B., Tinevez, J.-Y., White, D. J., Hartenstein, V., Eliceiri, K., Tomancak, P., and Cardona, A., 2012, Fiji: An open-source platform for biological-image analysis: Nature Methods, v. 9, p. 676–682.

Schindelin, J., Rueden, C. T., Hiner, M. C., and Eliceiri, K. W., 2015, The ImageJ ecosystem: An open platform for biomedical image analysis: Molecular Reproduction and Development, v. 82, p. 518–529, doi:10.1002/mrd.22489.

Schulze, P. C., Williamson, C. E., and Hargreaves, B. R., 1995, Evaluation of a remotely operated vehicle (ROV) as a tool for studying the distribution and abundance of zooplankton: Journal of Plankton Research, v. 17, p. 1233–1243, doi:10.1093/plankt/17.6.1233.

Spero, H. J., Lerche, I., and Williams, D. F., 1991, Opening the carbon isotope "vital effect" black box, 2, Quantitative model for interpreting foraminiferal carbon isotope data: Paleoceanography, v. 6, p. 639–655, doi:10.1029/91PA02022.

Spindler, M., Anderson, O. R., Hemleben, C., and Bé, A. W. H., 1978, Light and electron microscopic observations of gametogenesis in *Hastigerina pelagica* (Foraminifera): The Journal of Protozoology, v. 25, p. 427–433, doi:10.1111/j.1550-7408.1978.tb04164.x.

Spindler, M., Hemleben, C., Bayer, U., Bé, A. W. H., and Anderson, O. R., 1979, Lunar periodicity of reproduction in the planktonic foraminifer *Hastigerina pelagica*: Marine Ecology Progress Series, v. 1, p. 61–64.

Sun, G., and Krasnitz, A., 2014a, Significant distinct branches of hierarchical trees: A framework for statistical analysis and applications to biological data: BMC Genomics, v. 15, doi:10.1186/1471-2164-15-1000.

Sun, G., and Krasnitz, A., 2014b, TBEST: Tree Branches Evaluated Statistically for Tightness. Available from https://CRAN.R-project.org/package = TBEST

Swanberg, N. R., and Caron, D. A., 1991, Patterns of sarcodine feeding in epipelagic oceanic plankton: Journal of Plankton Research, v. 13, p. 287–312, doi:10.1093/plankt/13.2.287.

Tang, Y., Horikoshi, M., and Li, W., 2016, ggfortify: Unified interface to visualize statistical result of popular R packages: The R Journal, v. 8.2, p. 478–489.

Ward, J. H., 1963, Hierarchical grouping to optimize an objective function: Journal of the American Statistical Association, v. 58, p. 236–244, doi:10.1080/01621459.1963.10500845.

Weiner, A., Aurahs, R., Kurasawa, A., Kitazato, H., and Kucera, M., 2012, Vertical niche partitioning between cryptic sibling species of a cosmopolitan marine planktonic protist: Molecular Ecology, v. 21, p. 4063–4073, doi:10.1111/j.1365-294X.2012.05686.x.

Whitmore, B. M., Nickels, C. F., and Ohman, M. D., 2019, A comparison between *Zooglider* and shipboard net and acoustic mesozooplankton sensing systems: Journal of Plankton Research (in press).

Wickham, H., 2009, ggplot2: Elegant Graphics for Data Analysis. Available from https://www.springer.com/us/book/9780387981413

Zeebe, R. E., Bijma, J., and Wolf-Gladrow, D. A., 1999, A diffusion-reaction model of carbon isotope fractionation in foraminifera: Marine Chemistry, v. 64, p. 199–227, doi:10.1016/S0304-4203(98)00075-9.